A DMPs-Based Framework for Robot Learning and Generalization of Humanlike Variable Impedance Skills

Chenguang Yang, *Senior Member, IEEE*, Chao Zeng, Cheng Fang, *Member, IEEE*, Wei He, *Senior Member, IEEE*, and Zhijun Li, *Senior Member, IEEE*

***Abstract*—One promising approach for robots efficiently learning skills is to learn manipulation skills from human tutors by demonstration and then generalize these learned skills to complete new tasks. Traditional learning and generalization methods, however, have not well considered human impedance features, which makes the skills less humanlike and restricted in physical human–robot interaction scenarios. In particular, stiffness generalization has not been well considered. This paper develops a framework that enables the robot to learn both movement and stiffness features from the human tutor. To this end, the upper limb muscle activities of the human tutor are monitored to extract variable stiffness in real time, and the estimated human arm endpoint stiffness is properly mapped into the robot impedance controller. Then, a dynamic movement primitives model is extended and employed to simultaneously encode the movement trajectories and the stiffness profiles. In this way, both position trajectory and stiffness profile are considered for robot motion control in this paper to realize a more complete skill transfer process. More importantly, stiffness generalization and movement generalization can be efficiently realized by the proposed framework. Experimental tests have been performed on a dual-arm Baxter robot to verify the effectiveness of the proposed method.**

***Index Terms*—Dynamic movement primitives (DMPs), human–robot interaction, stiffness generalization, variable impedance skill transfer.**

Manuscript received October 22, 2017; revised January 28, 2018; accepted March 13, 2018. Date of publication March 20, 2018; date of current version June 12, 2018. Recommended by Technical Editor H. A. Varol. This work was supported in part by the National Natural Science Foundation of China under Grants 61473120, 61625303, 61751310, in part by the Science and Technology Planning Project of Guangzhou under Grant 201607010006, in part by the State Key Laboratory of Robotics and System (HIT) under Grant SKLRS-2017-KF-13, and in part by the Fundamental Research Funds for the Central Universities under Grant 2017ZD057. *(Corresponding author: Chenguang Yang.)*

C. Yang and C. Zeng are with the Key Laboratory of Autonomous Systems and Networked Control, College of Automation Science and Engineering, South China University of Technology, Guangzhou 510640, China (e-mail: cyang@ieee.org; mjzengchao@163.com).

C. Fang is with the Humanoids and Human Centered Mechatronics Lab, Istituto Italiano di Tecnologia, Genova 16163, Italy (e-mail: cheng.fang@iit.it).

W. He is with the School of Automation and Electrical Engineering, University of Science and Technology Beijing, Beijing 100083, China (e-mail: weihe@ieee.org).

Z. Li is with Department of Automation, University of Science and Technology of China, Hefei, 230026, China (email: zjli@ieee.org).

Color versions of one or more of the figures in this paper are available online at http://ieeexplore.ieee.org.

Digital Object Identifier 10.1109/TMECH.2018.2817589

I. Introduction

IT IS increasingly expected that robots are capable of flexible skills in order to adapt to more complex situations in physical human–robot interaction systems. Teaching by demonstration (TbD) [1], [2] is considered as one of the most effective ways for robots to learn motion and manipulation skills from humans. Conventional TbD methods, e.g., joysticks, keyboard, or human motion capture devices, have been more focused on fast programming for endpoint movement trajectory planning and control. Such interfaces may be efficient for simple tasks that depend only on position. However, they are hardly applicable for complicated interactions, especially when regarding scenarios where robots physically interact with the environment including humans and where stiffness profiles in addition to position trajectories need to be properly regulated [3]–[6].

Neuroscience studies have demonstrated how humans perform specific tasks by adapting limb muscle stiffness [7]. By using synthesized visual and haptic feedback, a human demonstrator is able to adjust his limb impedance to reduce the external interference under the control of the central nervous system. Variable impedance regulation widely exists in human task-performing cases. When performing a particular task, a human demonstrator could increase his limb force in a natural manner when the resistance force becomes larger, and vice versa. The impedance adaptive process plays a great role in such kinds of tasks. Similarly, adaptive impedance control is also necessary for robotic systems [8]–[10]. In our previous work [11]–[13], we have applied variable impedance skill transfer to robot skill learning scenarios. However, the work just focused on imitation learning, which refers to the process that the robot is only able to replay the learned motion skills exactly following what the human tutor has demonstrated. This paper further investigates the possibility for a robot to generalize the learned skills to new situations using a variable stiffness strategy.

Transferring human limb stiffness, which can be adjusted online in a real-time manner to a robot, is an effective way to realize variable impedance skill transfer [11], [14]–[16]. The electromyographic (EMG) signals extracted from human limbs contain rich information of muscle activities, based on which variation of human limb impedance can be effectively monitored and estimated during a task execution. Compared with the other methods [4], [6], [17], which take nonbiological ways to achieve

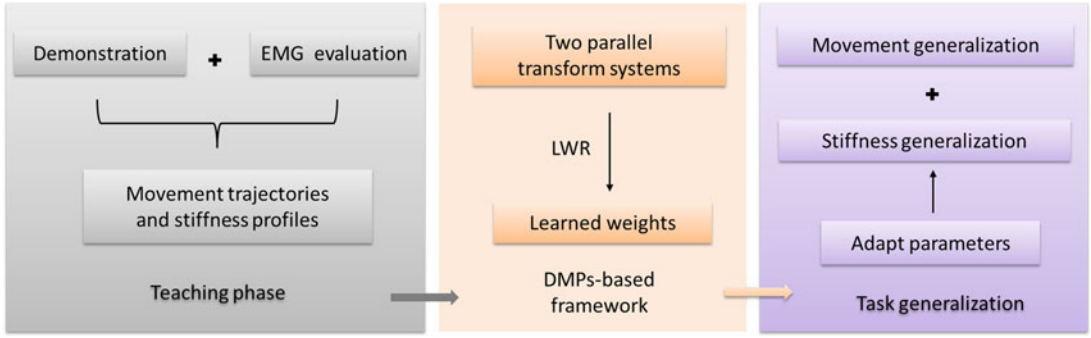

Fig. 1. Procedure of the developed TbD system for skills learning and generalization.

variable gains, the EMG-based method could allow the transfer of human impedance features to the robot. Therefore, the robot can adapt to complex tasks and environments in a more direct way [13].

In order to generalize skills obtained by imitation learning, movement trajectories need to be encoded such that they can be easily adapted to new situations. Dynamic movement primitives (DMPs) are one of the most commonly used methods to represent movements of humans and robots [18], [19]. The DMPs model is represented by a set of differential equations that can encode high-dimensional control policies. Thus far, several types of DMPs models have been developed and successfully utilized to learn a large number of skills such as ball-in-a-cup [20], drumming [20], and serving water [21]. However, these papers have only utilized the DMPs model to encode movement trajectories.

Recently, stiffness/force adaptation has been investigated based on this model. In [22], a DMPs method has been presented for variable stiffness scheduling, in which the gains are represented using a function approximator. In [23], a DMPs model is developed for the execution of bimanual or tightly coupled cooperative tasks by coupling force/torque feedback into the transform system. Steinmetz *et al.* [5] proposed a method to simultaneously transfer positional and force requirements for in-contact tasks. In [24], stiffness adaptation has been introduced to assist human tutor to increase the intuitiveness of interaction during teaching. Nemec *et al.* [25] proposed a method that enables stiffness adaptation in path operational space, considering the variance of motion across multiple executions and the current speed. These papers have verified the significance of stiffness/force adaptation for robot interactions with the environment including humans. However, it has not been investigated to model and learn the stiffness profiles in "muscle" space.

This paper proposes a framework that enables robots to efficiently learn both motor and stiffness control policies from humans. To that end, human limb muscle activities are monitored for variable stiffness estimation. The DMPs framework is extended to generalize movement trajectories and stiffness profiles. Additionally, a dual-arm control strategy with haptic feedback mechanism is developed for skill transfer. During the demonstration, the master arm of the robot is physically connected with the human tutor's hand and the slave arm follows the motion of the master arm through the attached virtual spring (see [13]). Finally, experimental studies are conducted to verify the approach on a Baxter robot. The whole framework is depicted in Fig. 1.

The main contributions of this paper can be summarized as follows: 1) This paper presents a scheme combining EMG-based variable impedance skill transfer with DMP-based motion sequence planning, inheriting the merits of these two aspects for robotic skill acquisition; and 2) more importantly, the developed framework can simultaneously encode both trajectories and stiffness profiles in a unified manner, which allows both trajectory generalization and stiffness schedule.

The rest of this paper is structured as follows. The methodology is first presented in Section II. The experimental evaluation is then presented in Section III. Finally, conclusion is given in Section IV.

II. Methodology

In this part, the EMG-based variable stiffness estimation method is introduced in Section II-A. Then, the teleoperation control strategy is developed for dual-arm imitation movement in Section II-B. In Section II-C, the DMPs framework for skill representation is finally presented.

A. EMG-Based Variable Stiffness Estimation

This modality is developed to enable the robot to learn a proper stiffness regulation strategy from the human tutor during demonstrations. To do so, the human tutor's limb endpoint stiffness is estimated first. The EMG signals extracted from the tutor's arm are used to monitor the muscle activation for the stiffness estimation. Subsequently, the estimated human endpoint stiffness profile is transferred to the robot as the gains in the joint impedance controller.

The conservative congruence transformation between the Cartesian stiffness and the stiffnesses of human arm is defined as follows [26]:

$$K_{\mathrm{en}} = J_h^{+T}(q_h)[K_j - \frac{\partial J_h^{+T}(q) F_{\mathrm{ex}}}{\partial q_h} \partial q_h] J_h^{+}(q_h) \qquad (1)$$

where $K_{\mathrm{en}} \in \mathbf{R}^{6\times6}$ and $K_j \in \mathbf{R}^{7\times7}$ are the human arm endpoint stiffness and joint stiffness, respectively. $J_h^{+T} \in \mathbf{R}^{6\times7}$ denotes

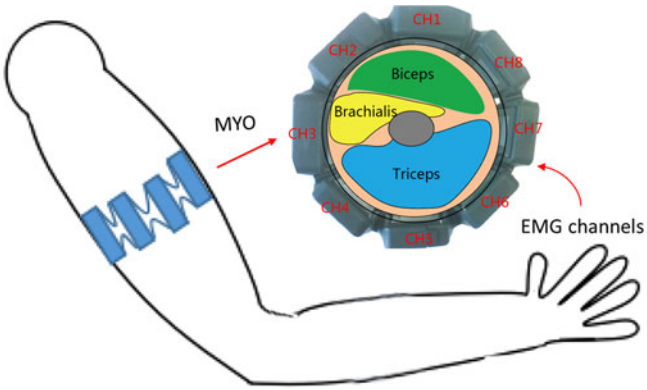

Fig. 2. Position of the eight-channel MYO for stiffness estimation.

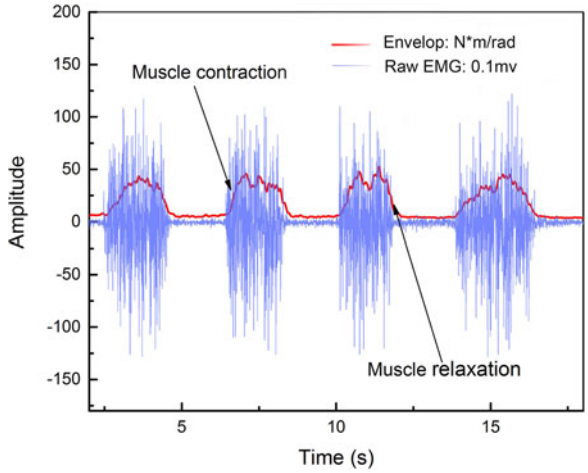

Fig. 3. Example of EMG enveloping by using a low-pass filter and moving average method. The blue line represents the raw EMG signals. The red line is the filtered stiffness coefficient representing limb muscle activities.

the pseudoinverse of the human arm Jacobian matrix, which represents the arm posture, and $q_h \in \mathbf{R}^7$ represents the arm joint angles. $F_{\text{ex}} \in \mathbf{R}^6$ is the external force that is applied at the human arm endpoint.

Generally speaking, the joint stiffness of human arm K_j is related to the muscle cocontraction activity, the posture of human arm, the muscle stretch reflex, etc. In this paper, a verified effective and simplified estimation model of human arm joint stiffness is employed [27], [28], where joint stiffness K_j is represented as multiplication of a muscle cocontraction indicator $\alpha(p)$ and an intrinsic constant stiffness $\overline{K_j}$, which can be identified at the condition of minimal muscle cocontractions, namely $K_j = \alpha(p)\overline{K_j}$. The coefficient $\alpha(p)$ can be obtained by

$$\alpha(p) = 1 + \frac{\lambda_1(1 - e^{-\lambda_2 p})}{(1 + e^{-\lambda_2 p})} \tag{2}$$

where λ_1 and λ_2 are positive constant coefficients to be estimated, and p is an indicator used to represent muscle activation level. The indicator p can be obtained in a two-step way: a low-pass filter (finite impulse response filter with a cutoff frequency of 100 Hz) and a moving average technique are first used to extract an envelope of the raw EMG signals from each of N channels using an EMG extraction device MYO. There are total $N = 8$ channels of the EMG signals used in this paper. MYO is worn on the upper arm to collect raw EMG data from the muscles, as shown in Fig. 2. An example of EMG envelope is shown in Fig. 3.

The moving average process takes the following equation:

$$f(A_t) = \frac{1}{W}\sum_{k=0}^{W-1} \text{EMG}(A_{t-k}) \tag{3}$$

where $f(A_t)$ represents the amplitude of the envelope, W represents the window size, which is set at 40 samples (at a sampling rate of 100 Hz). $\text{EMG}(A_k)$ indicates the amplitude of the raw EMG signal, which is detected from one channel. k and t are the sampling point and time, respectively. Then, the indicator p can be calculated by summing the absolute values of the amplitudes of the envelope of the EMG signals, as shown in the following equation [13]:

$$p = \sum_{i=1}^{N} |f_i(A_t)|. \tag{4}$$

Therefore, there are three parameters, i.e., the constant coefficients λ_1, λ_2, and the intrinsically constant joint stiffness matrix $\overline{K_j}$, that have to be estimated. These parameters can be estimated by minimizing the Frobenius norm of the following expression which is derived from (1):

$$\|\alpha(p)\overline{K_j} - \frac{\partial J_h^{+T}(q)F_{\text{ex}}}{\partial q_h} - J_h^T(q_h)\overline{K_{\text{en}}}J_h(q_h)\| \tag{5}$$

where the human arm Cartesian stiffness $\overline{K_{\text{en}}} \in \mathbf{R}^{6\times 6}$ can be identified in an indirect way [27].

The human arm Jacobian J_h is responsible for considering the geometrical change of the endpoint stiffness profile. To calculate J_h, a human arm kinematic model, i.e., the D–H model, is utilized to represent the simplified human arm kinematics (see [29] for details). It represents the human arm as a model with 7 degrees of freedom (DoFs) : 3 DoFs on the shoulder, 2 DoFs on the elbow, and 2 DoFs on the wrist. The calculation of the human arm joint angles is realized by measuring the quaternions obtained from two inertial measurement units, and then converting them to the joint angles according to [12].

B. Dual-Arm Control Strategy for Demonstration

A teleoperation-based kinesthetic teaching strategy is utilized for the realization of human-to-robot skills transfer in a teaching phase based on a dual-arm robot platform. A dual-arm control strategy is accordingly designed to achieve this goal. One of the two arms is used as the master arm and the other as the slave arm, and the master arm is connected to the human tutor's hand by using a mechanical coupling interface. The human tutor takes the master arm to move and the robot slave arm synchronously follows the motion to execute a specific task. Compared to the

traditional way of demonstration, in which the human tutor may hold and drive the slave arm directly, this indirect way of demonstration (teleoperation) can make the human tutor adapt his muscle activity and the corresponding Cartesian stiffness more naturally. This process can be considered as imitation learning.

A haptic feedback mechanism integrated into the dual-arm control is provided to the human tutor, which contributes to stimulating the human tutor's muscle activation for the stability improvement of the task execution. A virtual spring-damping system is attached between the robot two arms. The human tutor's hand is connected to the robot master arm using a mechanical interface [13]. The slave arm follows the motion of the master arm in both Cartesian space and joint space under the designed control mode. Due to the movement tracking error between the two arms, a virtual resistance force is generated as haptic feedback and provided to the human tutor. Thus, the tutor is able to "feel" the motion error in a real-time manner and can regulate his muscle strength to compensate for the error. We leave the detail of the dual-arm control strategy to [13].

C. Dynamical Movement Primitives for Skill Representation

In this section, the DMPs model learned from multiple demonstrations is first introduced for position trajectory adaptation. Furthermore, this DMPs framework is also extended for the stiffness adaptation.

1) DMPs for Trajectory Planning: Generally, DMPs models can be classified into two types, i.e., the $Discrete$ DMPs and the $Rhythmic$ DMPs with respect to different kinds of tasks. For the realization of the experimental task, i.e., the cutting task, the former type is used in this paper. A typical DMPs mode can be seen as a spring-damping system, which is derived by a canonical system. The model is defined as follows [18]–[19]:

$$\tau \dot{v} = k(g - x) - d\dot{x} + (g - x_0) f(s) \tag{6}$$

$$\tau \dot{x} = v \tag{7}$$

where x denotes the position of the robot endpoint or joint angle, and v is the velocity. k and d represent the spring and damping coefficients of the system, respectively. The positive constant τ is the temporal scaling coefficient. By adjusting the coefficient τ, duration of a task would be accordingly changed. x_0 and g denote the initial and goal position, respectively. The external force term $f(s)$ is a nonlinear continuous bounded function. s is the state of a first-order dynamic system, i.e., the canonical system, which shares the same temporal constant τ

$$\tau \dot{s} = -\alpha_s s, \quad s \in [0, 1]; \quad s(0) = 1 \tag{8}$$

where the predefined constant is represented by α_s.

The state s can be seen as a phase variable, which is set to monotonically decrease from 1 to 0. When s converges to zero, the external force term vanishes at the target point [see (9)]. Due to the canonical system, the DMPs model depends not on time but on the state s, which makes it possible to easily generalize the model to be suitable for other situations without changing the movement trajectory.

The nonlinear function $f(s)$ is defined by

$$f(s) = \sum_{i=1}^{N} \gamma_i \phi_i(s) s \tag{9}$$

with

$$\phi_i(s) = \frac{\exp(-h_i(s - c_i)^2)}{\sum_{j=1}^{N} \exp(-h_j(s - c_j)^2)} \tag{10}$$

where $\phi_i(s)$ is considered as a normalized radial basis function with the center c_i and the width h_i. Each basis function h_i is weighted by γ_i. N denotes the number of the Gaussian functions that need to be used in the model. The parameters c_i, h_i, and N are determined in accordance to the situation of a task.

A supervised learning process is needed for parameter estimation. Given a single demonstration, we obtain the target force $f_{\text{target}}(s)$ as follows:

$$f_{\text{target}}(s) = \frac{\tau \dot{v} + d\dot{x} - k(g - x)}{g - x_0}. \tag{11}$$

Then, the weights γ of DMPs model are calculated using locally weighted regression

$$\min \left(\sum \left(f_{\text{target}}(s) - f(s) \right)^2 \right). \tag{12}$$

There are three basic advantages of the DMPs model, which are follows:

1) the generated movement adapts to a new goal g with a smooth trajectory, which is similar to the original one; thus, the model is spatially generalized;
2) the model can be generalized in temporal dimension just by changing the temporal constant τ without affecting the shape of the movement trajectory; and
3) by adding coupling terms to the differential equation (6), the modified model is then able to have other abilities such as avoiding static or moving obstacles [21] and robustness to external perturbations [30].

2) DMPs for Stiffness Schedule: In [17], [22], and [31], the control policy K (i.e., the gain of the robot joint impedance controller) is represented by a function approximator

$$K = \sum_{i=1}^{M} \omega_i \varphi_i(s) \tag{13}$$

where $\varphi_i(s)$ are basis functions. ω_i are weighting parameters, which are calculated via a supervised learning algorithm and optimized via a reinforcement learning algorithm.

In fact, the function approximator is analogous to the force function, i.e., $f(s)$ in (9). Their framework only utilized a part of the DMPs model due to the lack of a reference stiffness profile that can be used for imitation learning. Therefore, it is only able to inherit parts of the merits of the DMPs model. There are three shortcomings of this framework, which are as follows.

1) The initial stiffness is set to be a constant value, and it needs a learning process for the robot to obtain a variable stiffness profile. Thus, their framework is not efficient in transferring skills from humans to a robot.

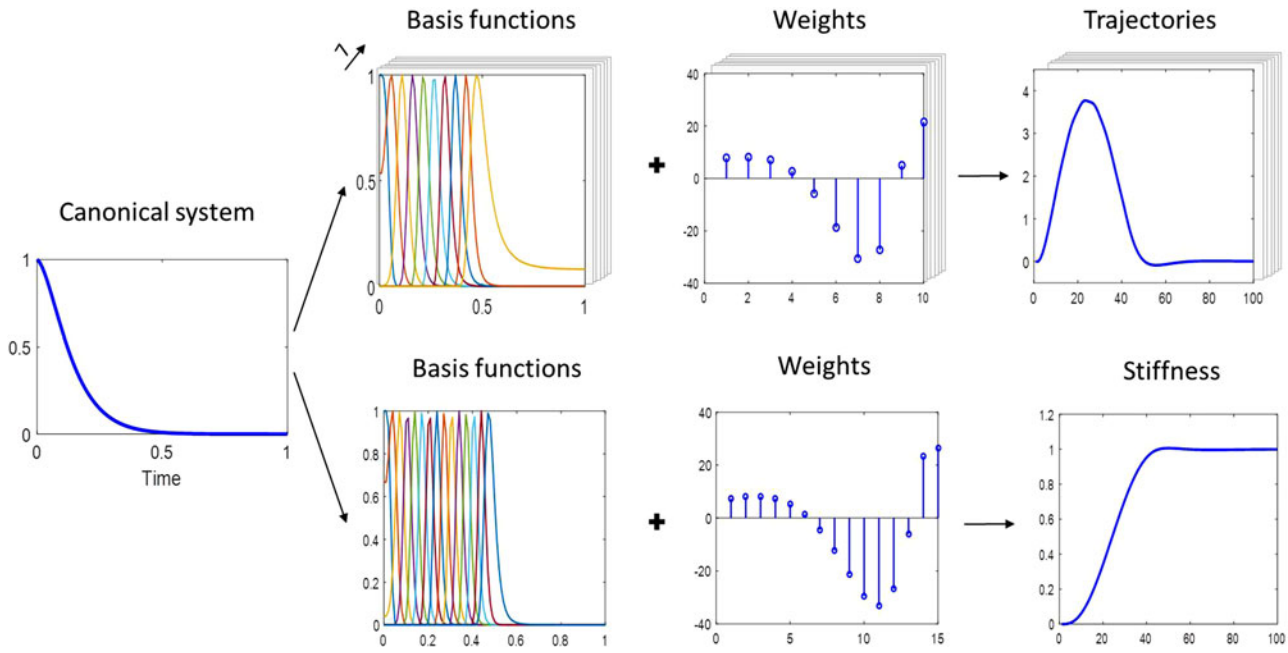

Fig. 4. Extended framework of the DMPs system. Two sets of transform systems are used to represent for position trajectories and stiffness profiles, respectively. The two systems are driven by the same canonical system using the same temporal scaling coefficient τ in order to satisfy phase synchronization.

2) The stiffness cannot be directly generalized to other situations, i.e., the amplitude and duration cannot be easily adjusted to suit for similar tasks with different requirements.
3) It is not allowed to be used in such scenarios where it only has one shot to finish a task because the trial-and-error process is needed to learn the stiffness. Taking the example of cutting, we would like the robot to cut an object in one time but not try several times to achieve a proper stiffness profile. Many similar examples can be found in industrial applications.

In order to overcome these shortcomings, we extend the framework in this paper based on the idea that a complete motion process of a robot should include both position trajectories and stiffness profiles. Robots, just like humans, should be capable of both trajectory adaptation and stiffness adaptation such that they are able to learn and generalize highly humanlike skills. To that end, representation of trajectories and stiffness profiles can be treated equally. Inspired by [19], our extended framework can be described as:

$$\dot{s} = h(s) \tag{14}$$

$$\dot{x} = g_1(x, s, \gamma) \tag{15}$$

$$\dot{p} = g_2(p, s, \omega) \tag{16}$$

where $h(s)$ is the canonical system and it is represented by (8). Equations (15) and (16) show the two transform systems that one is used to encode position trajectories and another one for stiffness profiles. The output of the stiffness DMPs model, i.e., $\Omega_i = \{p_i, \dot{p}_i\}$ is also obtained from (18). Note that these two transform systems are driven by the same canonical system such that the phase synchronization can be guaranteed. It means that the appropriate stiffness can be provided to the robot arm when it is needed. We use the notation p to represent the stiffness because the variable stiffness is evaluated from EMG signals and it can be seen as a stiffness indicator (see Section II-A). We compute the stiffness DMPs model using the indicator [see (4)] instead of the gains of all joints to reduce the computations.

The whole framework is demonstrated in Fig. 4 that is modified from [22]. The calculation procedure for stiffness DMPs is similar to the process of movement DMPs and only needs minor modifications, i.e., replacing the input x with p and choosing proper parameters, such as the spring and damping coefficients, and the number of basis functions.

To learn the weights from multiple demonstrations, we take a direct way to determine the weights. First, each demonstration is evaluated with a score of the scale from 1 to 10 according to its corresponding performance. For each demonstration, a coefficient κ_i is related to the scores π_i and defined as follows:

$$\kappa_i = \frac{\pi_i}{\sum_{i=1}^{L} \pi_i} \tag{17}$$

where L is the total number of the demonstrations. Then, the final DMPs output $\Omega = \{x, \dot{x}, p\}$ is computed as

$$\Omega = \sum_{i=1}^{L} \kappa_i \Omega_i. \tag{18}$$

Thus, the multiple demonstrations can be integrated together to yield a final output.

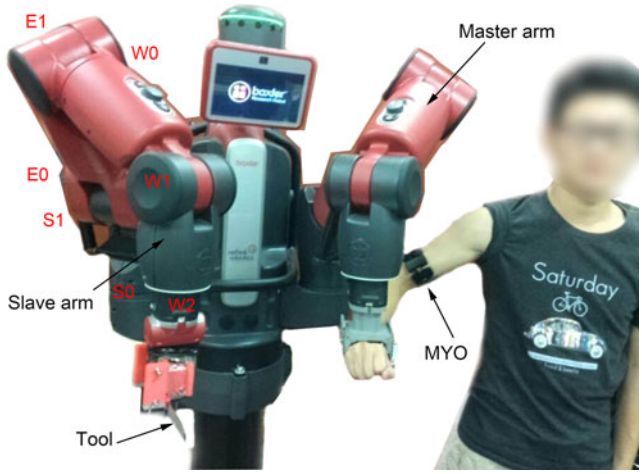

Fig. 5. Experimental setup for the cutting task during demonstration.

III. Experimental Evaluation

The humanoid dual-arm Baxter Research Robot (Baxter) developed by *Rethink Robotics* is used in our experimental study. Each arm of the robot has 7 DoF, i.e., 2-DoF shoulder joint (S0, S1), 2-DoF elbow joint (E0, E1), and 3-DoF wrist joint (W0, W1, W2). The kinematics model of the robot arm has been developed in the previous work [32]. Joint stiffness and damping can be modified under torque control mode, which is implemented by the proportion-derivative impedance control law. The human tutor's muscle activity is monitored using a MYO device to collect raw EMG signals. Two tasks, cutting and lift place, are illustrated to justify the effectiveness of the proposed method.

A. Cutting Task

The setup is shown in Fig. 5. During demonstration, one arm of the robot is used as the master arm, which is physically attached to the human tutor's limb endpoint through a specially designed coupling device [13]. The other arm serves as a slave arm, and a knife is mounted onto its endpoint as a cutting tool. In the teaching phase, the human tutor drives the master arm to move, and the slave arm follows the movement and learns the patterns of the position trajectory and the stiffness profile of the hand of the human tutor. While in the following reproduction phase, the slave arm is able to reproduce and generalize the learned skill without the assistance of the master arm.

First, in the teaching phase, the human tutor who has been involved in the stiffness calibration demonstrates the cutting skill through teleoperation ten times. The trajectories of the seven joints as well as the tutor's limb EMG signals are recorded during each demonstration. Note that the EMG signals can be evaluated in an almost real-time manner; thus, we can directly record the EMG data and calculate the stiffness indicator p.

Then, a direct way of computing the mixture of movement primitives [see (17) and (18)] is used to generate one output of the DMPs model based on the multiple demonstrations. Note that learning from multiple demonstrations is not the main concern of this paper. Therefore, a qualitative criterion is employed to determine the weight of each single demonstration. To that end, each one of the three subjects gives a score ranging from 1 to 10 for each signal demonstration according to the task execution performance. If the system is unstable when the slave arm contacts with the object or the object is not cut well eventually during the demonstration, it will get a lower score, the weights are calculated by using (17). One may also employ objective approaches for learning from multiple demonstrations (see, e.g., [33]).

The spring coefficient k and damping coefficient d of the DMPs model are set to 150 and 25, respectively. The numbers of basis functions are chosen: 100 and 50 for the trajectories DMPs and the stiffness DMPs, respectively. Once we achieve the generated movement trajectories and stiffness profiles that account for multiple demonstrations, the following two subtasks are conducted.

1) Movement Trajectory Planning Using the DMPs Model: In this subtask, we would like to extend the ability of DMPs model for skill spatial generalization from position control mode to impedance control mode. The goal is to generate the learned skill to cut an object in different spatial positions. In our case, it is designed to cut a cucumber in different positions along the y-axis. The robot here is controlled in the EMG-based variable impedance mode. Note that in position control mode, only paths need to be planned, whereas in impedance control mode, both the paths and velocities should be adjusted. The generalized trajectories and velocities are achieved just by changing the profile of the DMPs model, and they are shown in the $top\ row$ in Fig. 6. It demonstrates that the generalized trajectories are very similar to the reference ones but converging to different goals.

The results of this subtask are shown in the $bottom\ row$ in Fig. 6. Fig. 6(c) shows the measured endpoint position in y-axis of the robot slave arm. It demonstrates that the endpoint could generalize spatially to different positions. Fig. 6(d) shows the executed cuts. This subtask demonstrates that DMPs model for skill spatial generalization can be successfully realized in impedance control model.

2) Stiffness Schedule: One of the most important contribution of our proposed framework lies in the ability of generalizing the stiffness profiles to suit for new given situations. This subtask aims to demonstrate this point. To that end, we generalize the reference stiffness indicator (the reference terminal value is 0.65) to two different goals, e.g., 0.8 and 0.9, based on the extended DMPs model, which is shown in Fig. 7(a). A different object is used for cutting in this subtask, which has a thicker skin and larger hardness than the object used in the teaching phase and the subtask above.

The robot is required to perform the subtask five times under each one of the three conditions described above, resulting in a successful rate of 0/5, 1/5, and 5/5, respectively. Fig. 7(b)–(f) shows one typical result of this subtask. In this case, it shows that the object cannot be successfully cut using the impedance control mode with the reference variable stiffness. And when the final stiffness value is generalized to 0.8, the subtask still cannot be successfully finished. Until it is generalized to a higher value, i.e., 0.9, the object can be successfully cut. Note that there is a gap between the final positions of the reference and

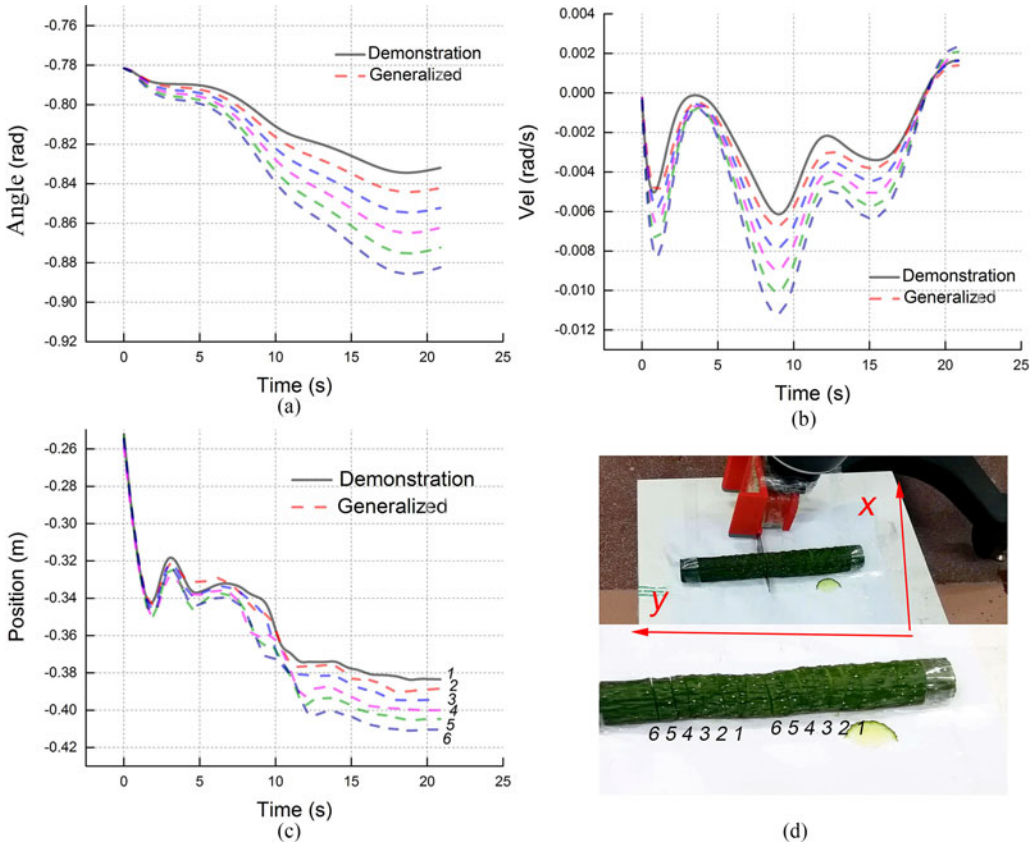

Fig. 6. Top: (a) and (b) are the planned trajectories for skill spatial generalization. $Bottom$: (c) is the measured robot endpoint position in y-axis; (d) shows the executed cut locations on the cucumber, two sets of numbers (1–6) mean this subtask is successfully performed twice (six cuts once). Cut no. 1 refers to the demonstrated one, and the others refer to the generalized ones. The solid lines denote the reference trajectories obtained from imitation learning and the dash lines denote the generalized ones.

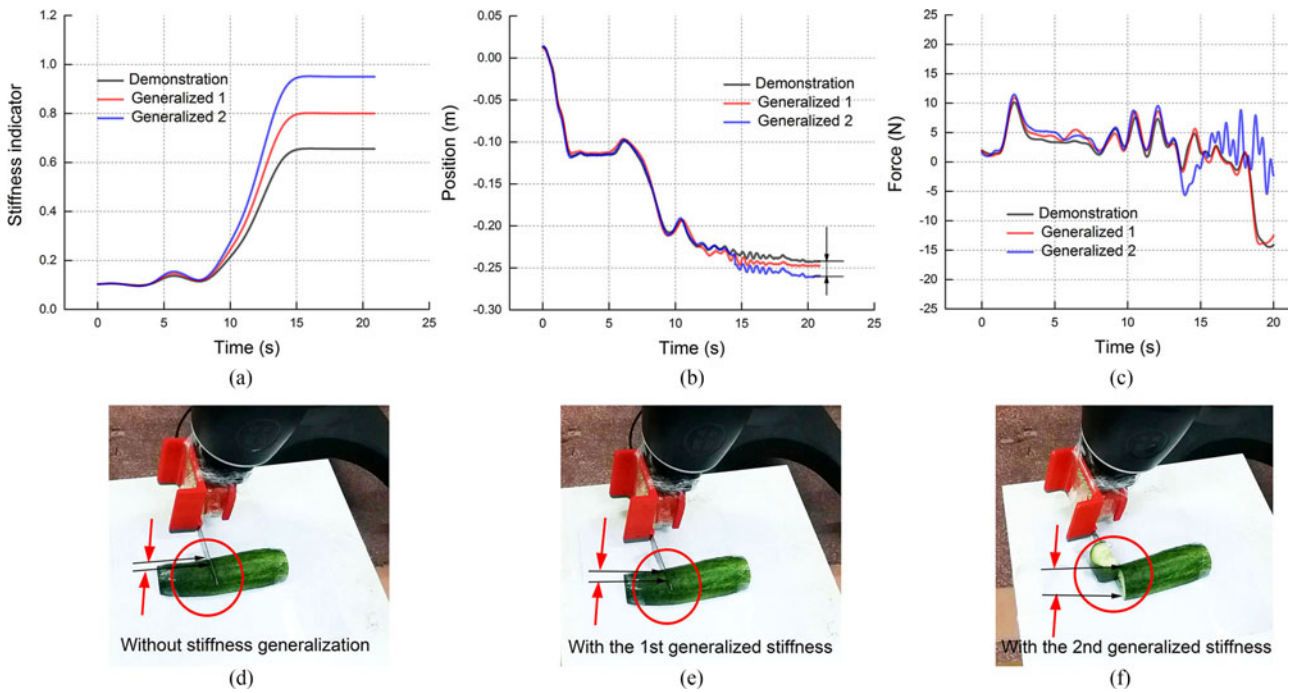

Fig. 7. Top : (a) is the generalization of the stiffness indicator profile to different goals. (b) and (c) are the measured positions and forces of the slave arm end-effector in *z*-axis, respectively. $Bottom$ shows the different cuts by using the reference (d), the first generalized (e), and the second generalized stiffness indicator profiles (f), respectively. The object can be cut successfully only by applying the second generalized stiffness profile. Note that the object used to cut here is different from the object used in the first subtask, as shown in Fig. 6.

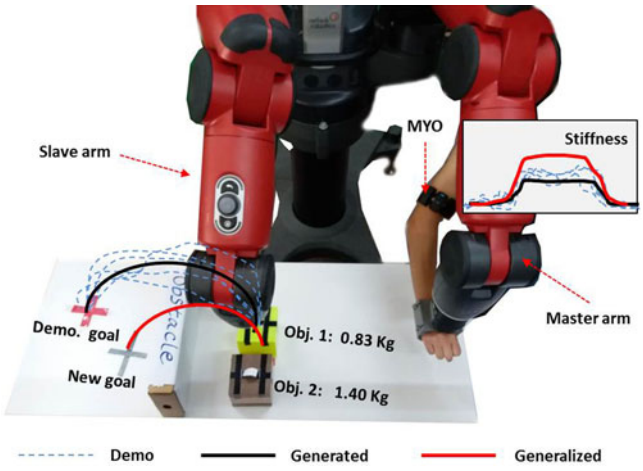

Fig. 8. Experimental setup for the lift-place task.

the second generalized trajectories, which represents the height of the object [see Fig. 7(b)]. From the perspective of force [see Fig. 7(c)], it can be seen that the robot lacks adaptability even in variable impedance control mode if the desirable stiffness profile is not properly generalized, which is consistent with our common experience when people perform tasks.

B. Lift-Place Task

The setup for the lift-place task is shown in Fig. 8. There are two different objects used in this task, objects 1 and 2 have the same size (10 cm $\times$10 cm $\times$ 10 cm), but different weights: 0.83 and 1.40 kg, respectively. The experimental procedure of this task is similar to the cutting task. During demonstration, the same human tutor teaches the robot to lift the object 1, pass over the obstacle (with a height of 18 cm), and finally place it on the goal (the red cross mark). The human tutor is required to lift the object at as low height as possible to pass it over the obstacle for energy saving. After a given number of demonstrations, we can generate one integrated position trajectory and one integrated stiffness profile, as shown in Fig. 9. The parameters of the DMP model are set as the same as in the cutting task.

During the playback phase, the robot is required to perform the task under three different situations: subtask 1: to lift and place the object 1 to a new given goal (the black cross mark), which is 5 cm away from the old one, with the demonstrated stiffness profile (i.e., trajectory spatial schedule); subtask 2: to lift and place the object 2 to the new given goal with the demonstrated stiffness profile (i.e., without stiffness schedule); and subtask 3: to lift and place the object 2 to the new goal with a generalized stiffness profile (i.e., both trajectory and stiffness generalization).

Each subtask has been performed seven times. A success rate of $7/7$ is obtained in the first subtask, which shows the skill spatial generalization has been successfully realized. The robot has finished the second task and the third subtask with a success rate of $1/7$ and $6/7$, respectively. The two comparative subtasks demonstrate the effectiveness of the proposed framework for stiffness schedule. Fig. 10 I–IV shows one typical example of the demonstrations and the three subtasks, respectively.

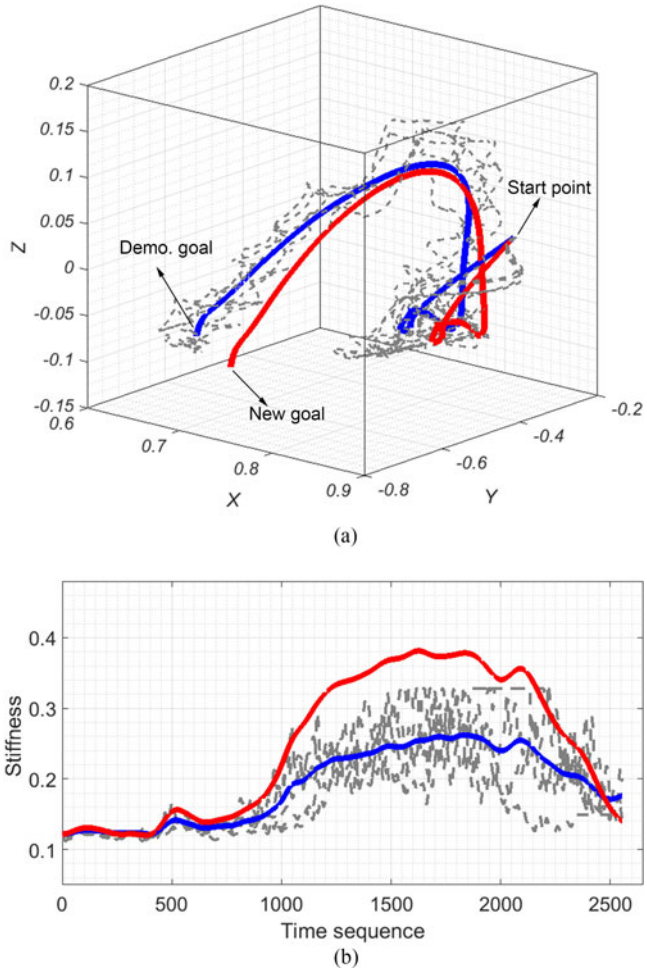

Fig. 9. Trajectories (a) and stiffness profiles (b) of the lift-place task.

C. Discussion

It should be emphasized that subtask 2 in Section III-A and subtask 3 in Section III-B are successfully performed just by adapting the parameters of the DMPs model instead of teaching the robot again or requiring additional time-consuming process (e.g., [22] and [34]) for achieving the proper stiffness profiles. Additionally, different combinations of the trajectories and the stiffness profiles can meet different requirements of task situations based on the proposed framework. More specifically, by combining different movement trajectories with the same stiffness profile, skill spatial generalization under variable impedance control mode can be realized (subtask 1 in Section III-A and subtask 1 in Section III-B), and by combining different stiffness profiles with the same movement trajectory, then stiffness schedule can be realized (subtask 2 in Section III-A), or both trajectories and stiffness profiles can be simultaneously achieved (subtask 3 in Section III-B). Furthermore, the DMP-based framework is model free and available for different robotic platforms.

The reference stiffness profile for stiffness generalization is obtained based on the extraction of the EMG signals and the subsequent calculation for the endpoint stiffness estimates. The human endpoint stiffness estimation method used in this pa-

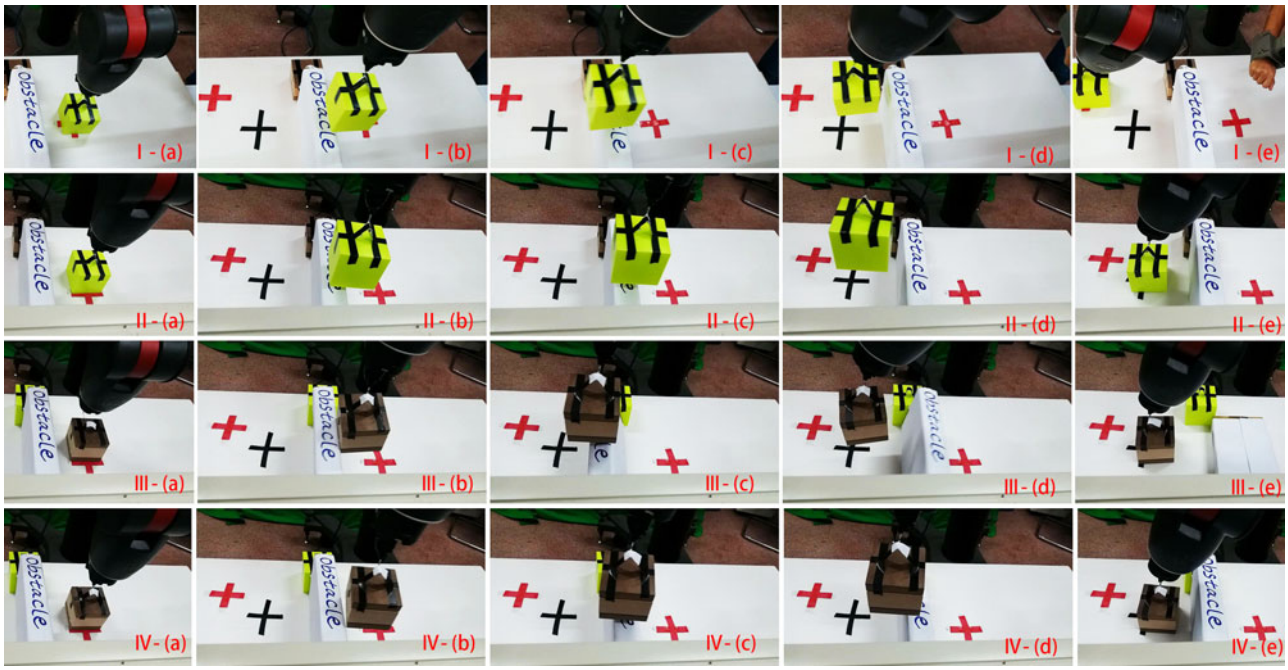

Fig. 10. Experimental results of the lift-place task: I-(a)–(e), II-(a)–(e), III-(a)–(e), and IV-(a)–(e) show one typical example of the demonstrations, subtask 1, subtask 2, and subtask 3, respectively. The robot fails to perform subtask 2.

per has been proved useful for impedance regulation in [27]. Therefore, on one hand, the stiffness transfer and generalization is achieved conveniently and efficiently; on the other hand, the reference stiffness profile largely depends on the accuracies of the extracted EMG signals and the stiffness estimation model. One may employ more complete stiffness estimation model to improve the accuracy of the estimated reference stiffness profile since the calculation efficiency of the estimation during the demonstration phase is not a strict constraint in this context.

Regarding the way, multiple demonstrations are used to generate a reference trajectory and a stiffness profile (see Fig. 9). The weight of each single demonstration is determined in a qualitative way for simplicity. Other more objective methods such as probabilistic movement primitives (e.g., [35]) can be utilized to achieve the same purpose. Moreover, different human tutors have different demonstrations during the skill transfer process. Thus, it may help robots to achieve a better performance of executing tasks by considering the variance between different humans, namely learning from different human tutors.

The significance of stiffness adaptation for human-to-robot skill transfer has been verified in [13]. The stiffness adaptive process of the cutting task and the lift-place task can be seen in Figs. 7(a) and 9(b), respectively. This paper introduces the capability of stiffness generalization, and therefore enriches the diversity of the human-to-robot variable impedance transfer. In our tasks, the stiffness generalization refers to the regulation of the stiffness profile according to the task requirement. Taking, for example, the lift-place task, during the reaching step the stiffness is expected to remain small, and it increases when larger stiffness is required to lift a heavier object. Surely, it can be decreased accordingly as shown in Fig. 9(b).

IV. Conclusion

We presented a novel framework for learning and generalizing humanlike variable impedance skills. The goal was to enable a robot to be capable of performing tasks in a humanlike way. The merits of the EMG-based variable impedance control and the DMP model were integrated into our method for human–robot skills transfer. To do so, the human tutor's upper limb EMG signals were extracted to capture his muscle stiffness features. The estimated endpoint stiffness profiles then served as variable gains in the impedance controller. In this way, the human tutor is able to naturally and intuitively transfer his impedance features of a specific skill to the robot. The DMP framework was employed and extended for both trajectory and stiffness schedule. It is worth noting that the stiffness planning and generalization for skill transfer can be achieved using our proposed framework, which is the first time to be reported in the literature to the best of our knowledge.

The proposed framework was evaluated on a real robot with multiple DoFs. The experimental results of the cutting and lift-place tasks have demonstrated the effectiveness of the proposed framework. It should be also mentioned that our method can be easily transplanted to other platforms, and this proposed framework can also be applied to a number of potential applications, such as industrial robots, robotic exoskeletons, and medical robotic systems, which are required to acquire humanlike manipulation skills.

In the future work, we will apply our method to perform more complex tasks. For example, it can be applied to a human–robot collaboration scenario, for instance a wood sawing task is performed by a robot and a human collaborator (similar to [15]). In these situations, research on the coordinated mechanism for both movement generalization and stiffness scheduling would

be essential. Furthermore, the stiffness scheduling mechanism we established here can be combined with many other trajectory expression tools, such as Gaussian mixture model, together to achieve variable impedance control for robots, which could enrich the diversity of the skills that robots are able to learn.

Acknowledgment

The authors would like to thank the editors and the anonymous reviewers for their insightful comments that helped them to improve the quality of this paper.

References

[1] A. Billard, S. Calinon, R. Dillmann, and S. Schaal, "Robot programming by demonstration," in *Springer Handbook of Robotics*. New York, NY, USA: Springer, 2008, pp. 1371–1394.

[2] S. Calinon, *Robot Programming by Demonstration*. Lausanne, Switzerland: EPFL Press, 2009.

[3] P. Kormushev, S. Calinon, and D. G. Caldwell, "Imitation learning of positional and force skills demonstrated via kinesthetic teaching and haptic input," *Adv. Robot.*, vol. 25, no. 5, pp. 581–603, 2011.

[4] L. Rozo, S. Calinon, D. G. Caldwell, P. Jimenez, and C. Torras, "Learning collaborative impedance-based robot behaviors," *AAAI Conf. Artificial Intell.*, Bellevue, WA, USA, 2013, pp. 1422–1428.

[5] F. Steinmetz, A. Montebelli, and V. Kyrki, "Simultaneous kinesthetic teaching of positional and force requirements for sequential in-contact tasks," in *Proc. 2015 IEEE-RAS 15th Int. Conf. Humanoid Robots (Humanoids)*, Nov. 2015, pp. 202–209.

[6] L. Rozo, S. Calinon, D. G. Caldwell, P. Jimenez, and C. Torras, "Learning physical collaborative robot behaviors from human demonstrations," *IEEE Trans. Robot.*, vol. 32, no. 3, pp. 513–527, Jun. 2016.

[7] E. Burdet, R. Osu, D. W. Franklin, T. E. Milner, and M. Kawato, "The central nervous system stabilizes unstable dynamics by learning optimal impedance," *Nature*, vol. 414, no. 6862, pp. 446–449, 2001.

[8] M. Howard, D. J. Braun, and S. Vijayakumar, "Transferring human impedance behavior to heterogeneous variable impedance actuators," *IEEE Trans. Robot.*, vol. 29, no. 4, pp. 847–862, Aug. 2013.

[9] F. Ficuciello, L. Villani, and B. Siciliano, "Variable impedance control of redundant manipulators for intuitive human–robot physical interaction," *IEEE Trans. Robot.*, vol. 31, no. 4, pp. 850–863, Aug. 2015.

[10] W. He and Y. Dong, "Adaptive fuzzy neural network control for a constrained robot using impedance learning," *IEEE Trans. Neural Netw. Learn. Syst.*, vol. 29, no. 4, pp. 1174–1186, Apr. 2018.

[11] P. Liang, C. Yang, N. Wang, Z. Li, R. Li, and E. Burdet, "Implementation and test of human-operated and human-like adaptive impedance controls on Baxter robot," in *Advances in Autonomous Robotics Systems*. New York, NY, USA: Springer, 2014, pp. 109–119.

[12] C. Yang, P. Liang, A. Ajoudani, Z. Li, and A. Bicchi, "Development of a robotic teaching interface for human to human skill transfer," in *Proc. 2016 IEEE/RSJ Int. Conf. Intell. Robots Syst.*, Oct. 2016, pp. 710–716.

[13] C. Yang, C. Zeng, P. Liang, Z. Li, R. Li, and C. Y. Su, "Interface design of a physical human-robot interaction system for human impedance adaptive skill transfer," *IEEE Trans. Autom. Sci. Eng.*, vol. 15, no. 1, pp. 329–340, Jan. 2018.

[14] B. Yuan, M. Sekine, J. Gonzalez, J. Tames, W. Yu, and B. Yuan, "Variable impedance control based on impedance estimation model with EMG signals during extension and flexion tasks for a lower limb rehabilitation robotic system," *J. Novel Physiotherapies*, vol. 3, no. 178, p. 2, 2013. [Online]. Available: https://www.omicsonline.org/open-access/variable-impedance-control-based-on-impedance-estimation-model-with-emg-signals-during-extension-and-flexion-tasks-for-a-lower-limb-rehabilitation-robotic-system-2165-7025-178.php?aid=19135

[15] L. Peternel, T. Petrič, E. Oztop, and J. Babič, "Teaching robots to cooperate with humans in dynamic manipulation tasks based on multi-modal human-in-the-loop approach," *Auton. Robots*, vol. 36, no. 1–2, pp. 123–136, 2014.

[16] A. Ajoudani, *Transferring Human Impedance Regulation Skills to Robots*, vol. 110. New York, NY, USA: Springer, 2016.

[17] J. Buchli, F. Stulp, E. Theodorou, and S. Schaal, "Learning variable impedance control," *Int. J. Robot. Res.*, vol. 30, no. 7, pp. 820–833, 2011.

[18] S. Schaal, P. Mohajerian, and A. Ijspeert, "Dynamics systems vs. optimal control—A unifying view," *Prog. Brain Res.*, vol. 165, pp. 425–445, 2007.

[19] A. J. Ijspeert, J. Nakanishi, H. Hoffmann, P. Pastor, and S. Schaal, "Dynamical movement primitives: Learning attractor models for motor behaviors," *Neural Comput.*, vol. 25, no. 2, pp. 328–373, 2013.

[20] A. Ude, A. Gams, T. Asfour, and J. Morimoto, "Task-specific generalization of discrete and periodic dynamic movement primitives," *IEEE Trans. Robot.*, vol. 26, no. 5, pp. 800–815, Oct. 2010.

[21] H. Hoffmann, P. Pastor, D. H. Park, and S. Schaal, "Biologically-inspired dynamical systems for movement generation: Automatic real-time goal adaptation and obstacle avoidance," in *Proc. 2009 IEEE Int. Conf. Robot. Autom.*, May 2009, pp. 2587–2592.

[22] F. Stulp, J. Buchli, A. Ellmer, M. Mistry, E. A. Theodorou, and S. Schaal, "Model-free reinforcement learning of impedance control in stochastic environments," *IEEE Trans. Auton. Mental Develop.*, vol. 4, no. 4, pp. 330–341, Dec. 2012.

[23] A. Gams, B. Nemec, A. J. Ijspeert, and A. Ude, "Coupling movement primitives: Interaction with the environment and bimanual tasks," *IEEE Trans. Robot.*, vol. 30, no. 4, pp. 816–830, Aug. 2014.

[24] M. Tykal, A. Montebelli, and V. Kyrki, "Incrementally assisted kinesthetic teaching for programming by demonstration," in *Proc. 11th ACM/IEEE Int. Conf. Human–Robot Interaction*, 2016, pp. 205–212.

[25] B. Nemec, N. Likar, A. Gams, and A. Ude, "Human robot cooperation with compliance adaptation along the motion trajectory," *Auton. Robots*, pp. 1–13, 2017. [Online]. Available: https://link.springer.com/article/10.1007/s10514-017-9676-3

[26] S.-F. Chen and I. Kao, "Conservative congruence transformation for joint and Cartesian stiffness matrices of robotic hands and fingers," *Int. J. Robot. Res.*, vol. 19, no. 9, pp. 835–847, 2000.

[27] A. Ajoudani, N. Tsagarakis, and A. Bicchi, "Tele-impedance: Teleoperation with impedance regulation using a body–machine interface," *Int. J. Robot. Res.*, vol. 31, no. 13, pp. 1642–1656, 2012.

[28] A. Ajoudani, C. Fang, N. G. Tsagarakis, and A. Bicchi, "A reduced-complexity description of arm endpoint stiffness with applications to teleimpedance control," in *Proc. 2015 IEEE/RSJ Int. Conf. Intell. Robots Syst.*, Sep. 2015, pp. 1017–1023.

[29] X. Ding and C. Fang, "A novel method of motion planning for an anthropomorphic arm based on movement primitives," *IEEE/ASME Trans. Mechatronics*, vol. 18, no. 2, pp. 624–636, Apr. 2013.

[30] J. Kober, B. Mohler, and J. Peters, "Learning perceptual coupling for motor primitives," in *Proc. 2008 IEEE/RSJ Int. Conf. Intell. Robots. Syst.*, Sep. 2008, pp. 834–839.

[31] L. Zhijun, T. Zhao, F. Chen, Y. Hu, C.-Y. Su, and T. Fukuda, "Reinforcement learning of manipulation and grasping using dynamical movement primitives for a humanoid-like mobile manipulator," *IEEE/ASME Trans. Mechatronics*, vol. 23, no. 1, pp. 121–131, Feb. 2018.

[32] Z. Ju, C. Yang, and H. Ma, "Kinematics modeling and experimental verification of Baxter robot," in *Proc. 33rd Chin. Control Conf.*, Jul. 2014, pp. 8518–8523.

[33] S. Calinon, F. D'halluin, D. G. Caldwell, and A. G. Billard, "Handling of multiple constraints and motion alternatives in a robot programming by demonstration framework," in *Proc. 2009 9th IEEE-RAS Int. Conf. Humanoid Robots*, Dec. 2009, pp. 582–588.

[34] K. Kronander, M. Khansari, and A. Billard, "Incremental motion learning with locally modulated dynamical systems," *Robot. Auton. Syst.*, vol. 70, pp. 52–62, 2015.

[35] A. Paraschos, E. Rueckert, J. Peters, and G. Neumann, "Model-free probabilistic movement primitives for physical interaction," in *Proc. 2015 IEEE/RSJ Int. Conf. Intell. Robots. Syst.*, Sep. 2015, pp. 2860–2866.

Chenguang Yang (M'10–SM'16) received the B.Eng. degree in measurement and control from Northwestern Polytechnical University, Xi'an, China, in 2005, and the Ph.D. degree in control engineering from the National University of Singapore, Singapore, in 2010.

He received postdoctoral training at Imperial College London, London, U.K. His research interests include robotics and automation.

Dr. Yang is a recipient of the Best Paper Award from the IEEE Transactions on Robotics and a number of international conferences.

Chao Zeng received the M.S. degree in precision instruments and mechanics from Shanghai University, Shanghai, China, in 2016. He is currently working toward the Ph.D. degree in pattern recognition and intelligent system at the College of Automation Science and Engineering, South China University of Technology, Guangzhou, China.

His research interests include human–robot interaction, programming by demonstration, and human–robot skill transfers.

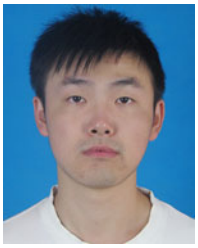

Cheng Fang (M'17) received the Ph.D. degree in mechanical design and theory from the Robotics Research Institute, Beihang University, Beijing, China, in 2013.

He is currently a Postdoctoral Researcher with the Humanoids and Human Centered Mechatronics Lab, Italian Institute of Technology, Genoa, Italy. His research interests include human–robot interaction, musculoskeletal modeling of human body, and task-motion planning and control of anthropomorphic arms.

Wei He (M'12–SM'16) received his B.Eng. and his M.Eng. degrees both in control theory and engineering from College of Automation Science and Engineering, South China University of Technology (SCUT), China, in 2006 and 2008, respectively, and his PhD degree in electrical and computer engineering from Department of Electrical & Computer Engineering, the National University of Singapore (NUS), Singapore, in 2011. He is currently working as a full professor in School of Automation and Electrical Engineering, University of Science and Technology Beijing, Beijing, China. He has co-authored 2 book published in Springer and published over 100 international journal and conference papers. He has been awarded a Newton Advanced Fellowship from the Royal Society, UK. He is a recipient of the IEEE SMC Society Andrew P. Sage Best Transactions Paper Award in 2017. He serves as an Associate Editor of *IEEE Transactions on Neural Networks and Learning Systems*, *IEEE Transactions on Control Systems Technology, IEEE Transactions on Systems, Man, and Cybernetics: Systems* and *IEEE Access*, and an Editor of *IEEE/CAA Journal of Automatica Sinica*, *Neurocomputing*, and *Journal of Intelligent & Robotic Systems*. He is the member of the IFAC TC on Distributed Parameter Systems, IFAC TC on Computational Intelligence in Control and IEEE CSS TC on Distributed Parameter Systems. His current research interests include robotics, distributed parameter systems and intelligent control systems.

Zhijun Li (M'07–SM'09) received the Ph.D. degree in mechatronics from Shanghai Jiao Tong University, Shanghai, China, in 2002.

From 2003 to 2005, he was a Postdoctoral Fellow with the Department of Mechanical Engineering and Intelligent Systems, University of Electro-Communications, Tokyo, Japan. From 2005 to 2006, he was a Research Fellow with the Department of Electrical and Computer Engineering, National University of Singapore, Singapore, and Nanyang Technological University, Singapore. Since 2012, he has been a Professor with the College of Automation Science and Engineering, South China University of Technology, Guangzhou, China. His research interests include service robotics, teleoperation systems, nonlinear control, neural network optimization, etc.

Dr. Li has been the Co-Chair of the Technical Committee on Biomechatronics and Biorobotics Systems of the IEEE Systems, Man and Cybernetics Society, and the Technical Committee on Neuro-Robotics Systems of the IEEE Robotics and Automation Society, since 2016. He is an Editor-at-Large for the *Journal of Intelligent and Robotic Systems*, and an Associate Editor for several IEEE transactions. He was the General Chair and Program Chair of 2016 and 2017 IEEE Conference on Advanced Robotics and Mechatronics, respectively.